

College of Engineering



Drexel E-Repository and Archive (iDEA)

<http://idea.library.drexel.edu/>

Drexel University Libraries

www.library.drexel.edu

The following item is made available as a courtesy to scholars by the author(s) and Drexel University Library and may contain materials and content, including computer code and tags, artwork, text, graphics, images, and illustrations (Material) which may be protected by copyright law. Unless otherwise noted, the Material is made available for non profit and educational purposes, such as research, teaching and private study. For these limited purposes, you may reproduce (print, download or make copies) the Material without prior permission. All copies must include any copyright notice originally included with the Material. **You must seek permission from the authors or copyright owners for all uses that are not allowed by fair use and other provisions of the U.S. Copyright Law.** The responsibility for making an independent legal assessment and securing any necessary permission rests with persons desiring to reproduce or use the Material.

Please direct questions to archives@drexel.edu

Determination of unknown stress states in silicon wafers using microlaser Raman spectroscopy

S. Narayanan and Surya R. Kalidindi

Department of Materials Engineering, Drexel University, Philadelphia, Pennsylvania 19104

Linda S. Schadler^{a)}

Department of Materials Science and Engineering, Rensselaer Polytechnic Institute, Troy, New York 12180

(Received 5 September 1996; accepted for publication 4 June 1997)

A new technique was developed to predict the unknown in-plane stress state and the magnitude of the stress components in (111) silicon wafers using micro-Raman spectroscopy. The approach is based on analyzing the combined signal from the initially degenerate peaks of the F_{2g} mode in silicon as a function of the angle between the incident laser polarization and the polarization selected from the scattered beam using an analyzer. The peak position of the combined signal when plotted as a function of the angle was found to contain the information required to estimate the magnitude of the individual stress components in the plane-stress condition. The development of this technique is described in this paper for (111) silicon wafers. © 1997 American Institute of Physics. [S0021-8979(97)09017-8]

I. INTRODUCTION

The Raman effect refers to the inelastic scattering of incident monochromatic light due to its interaction with the inherent atomic vibrations in a material.¹ The scattering results in a frequency shift of the incident light, and a spectral analysis of the scattered light reveals peaks that are uniquely dependent on the crystal geometry of the material being probed. The peaks are referred to as Raman peaks and the difference between the frequency of the incident light, and the frequency corresponding to the Raman peak is called the Raman frequency (expressed in wave numbers by convention). In recent years, micro-Raman spectroscopy (MRS) (which is Raman spectroscopy used to probe an area of the order of a few microns on the sample surface) has been used to measure surface stresses in crystalline solids by monitoring the modulation of Raman frequencies with externally applied loads.² The inelastically scattered light from the sample surface is usually comprised of multiple Raman frequencies with varying levels of degeneracy for each vibrational mode.

The most common procedure used in MRS stress measurements is to assume a stress state, monitor the shift in the Raman peak(s) with the magnitude of the applied stress (or strain), and generate a calibration curve of Raman peak position against the magnitude of the applied stress. This information is then used to measure the magnitude of stress on the same material in other loading situations.²⁻¹⁰ This technique has been used successfully in many systems: silicon,²⁻⁶ layered semiconductors,⁷ graphite-epoxy composites,⁸ aramid-epoxy composites,⁹ and graphite-glass composites.¹⁰ The major limitation of this technique is that the calibration curve is very sensitive to the stress state (e.g., tensile loading versus shear loading) and the lattice orientation of the crystal in the scatter volume. Furthermore, in many of the reported studies,⁸⁻¹⁰ the loss of degeneracy and the individual shifts of degenerate modes are ignored; only an "overall" shift of

the Raman signal for a given mode is measured and used in the calibration curves.

As an improvement, some researchers have isolated the initially degenerate peaks and measured individual peak shifts by using specific polarization conditions. Anastassakis *et al.*¹¹ showed that it is sometimes possible to isolate the initially degenerate peaks in the scattered light for a given crystal orientation and loading condition by proper selection of the incident laser polarization and the angle of the analyzer with respect to the sample orientation. These authors showed that uniaxial loading of a silicon cube along the $\langle 100 \rangle$ or $\langle 111 \rangle$ directions causes the initially triply degenerate F_{2g} mode in silicon to split into a singlet and a doublet, which can be observed independently by selecting the transverse and longitudinal polarizations in the scattered beam, respectively. They also demonstrated that both the singlet and the doublet shift by different amounts with the applied stress. This method has been used to determine uniaxial stresses and interfacial stresses in electronic components and layered structures.^{7,12}

The major limitation in attempting to isolate the peaks by selecting the polarization of the incident and scattered light is the need to know the stress state. In other words, the ratios of all the stress components have to be known beforehand, leaving only the magnitude of the stress tensor as unknown. Even if this limitation is overcome, it may not be feasible to find the proper polarization conditions for all loading conditions. For example, in shear loading of a silicon crystal in the $\langle 110 \rangle$ direction on the (111) plane, the initially triply degenerate F_{2g} mode splits into three singlets with overlapping peaks that cannot be isolated in the commonly used backscattered geometry under any polarization condition. Alternatively, one can try to isolate the overlapping peaks in the scattered light by mathematical analysis of the Raman spectra. For successful separation of the overlapping peaks and reliable estimation of their positions through mathematical analysis, the peaks have to be separated by at least four-tenths of the full width at half-maximum

^{a)}Electronic mail: schadl@rpi.edu

(FWHM).¹³ This condition is not met for the typical stresses encountered in silicon wafers for the F_{2g} mode, and therefore this option is not practical.

Recently, there have been attempts to extend the MRS technique with polarization selection rules to other material systems, such as SiC/Al composites,¹⁴ Nicalon/borosilicate glass composites,¹⁵ and graphite/epoxy composites.¹⁶ Sakata *et al.*¹⁶ studied the E_{2g} mode in axial loading of graphite fibers and reported two different slopes for the Raman peak shift with applied stress when the incident beam was polarized parallel and perpendicular to the loading direction, respectively. It is not clear if they have managed to isolate the two initially degenerate modes in this process or if the scattered light in these measurements is still comprised of overlapping E_{2g} mode peaks.

The goal of this investigation is to establish a procedure for using MRS to measure an unknown plane-stress state (with all three stress components being completely unknown) in silicon wafers of given crystallographic orientations. Silicon wafers were chosen for this study because the Raman effect in silicon is well characterized in the literature.² The plane-stress state assumption is appropriate because the wafers under investigation are thin and the measurements are from the sample surface. Instead of trying to isolate the individual shifts of the initially degenerate peaks using the polarization selection rules, this study endeavors to measure and use the information from the overall shift in the frequency of a given mode as a function of the relative angle between the polarization of the incident and scattered light. This information has been found to be adequate to predict a completely unknown plane stress state in the wafer. The theoretical development of this technique is presented in this paper for a (111) silicon wafer.

II. BACKGROUND

The theory behind the Raman effect and its modulation by external loads is described in many excellent review papers.^{2,17} These papers also describe the computations required to predict the peak shifts (including those that are initially degenerate) caused by any applied stress, provided the material parameters are known. Furthermore, for any given polarization condition, it is possible to theoretically predict the relative intensities of the different peaks in the scattered light. The details of these computations that are relevant to the development of our proposed technique are summarized here. This discussion will pertain only to the F_{2g} mode in silicon. The various steps involved in these calculations are as follows:

(1) The applied stress in the laboratory reference frame $[\sigma]_G$ is transformed to the crystal reference frame $[\sigma]_C$ using coordinate transformation laws

$$[\sigma]_C = [Q][\sigma]_G[Q]^T, \quad (1)$$

where $[Q]$ is the rotation matrix describing the transformation from the laboratory reference frame to the crystal reference frame.

(2) The strains in the crystal reference frame are obtained from the stresses in the crystal reference frame using linear elastic stress-strain relationships. In the standard contracted notation, this relationship for cubic crystals is usually expressed as

$$\begin{Bmatrix} \epsilon_{11} \\ \epsilon_{22} \\ \epsilon_{33} \\ 2\epsilon_{23} \\ 2\epsilon_{13} \\ 2\epsilon_{12} \end{Bmatrix}_C = \begin{bmatrix} S_{11} & S_{12} & S_{12} & 0 & 0 & 0 \\ S_{12} & S_{11} & S_{12} & 0 & 0 & 0 \\ S_{12} & S_{12} & S_{11} & 0 & 0 & 0 \\ 0 & 0 & 0 & S_{44} & 0 & 0 \\ 0 & 0 & 0 & 0 & S_{44} & 0 \\ 0 & 0 & 0 & 0 & 0 & S_{44} \end{bmatrix} \begin{Bmatrix} \sigma_{11} \\ \sigma_{22} \\ \sigma_{33} \\ \sigma_{23} \\ \sigma_{13} \\ \sigma_{12} \end{Bmatrix}_C, \quad (2)$$

where S_{11} , S_{12} , and S_{44} represent the elastic compliance parameters. The values of these parameters for silicon have been reported¹⁸ as $S_{11} = 7.68 \times 10^{-6}(\text{MPa})^{-1}$, $S_{12} = -2.14 \times 10^{-6}(\text{MPa})^{-1}$, and $S_{44} = 12.7 \times 10^{-6}(\text{MPa})^{-1}$.

(3) Each vibrational mode j is associated with a frequency ω_j and an effective force constant K_j^0 which is the second derivative of the crystal potential energy with respect to the mode normal coordinates where

$$K_j^0 \propto \omega_j^2 \quad (3)$$

in the absence of an externally imposed stress or strain on the crystal.

Due to the anharmonic nature of atomic interactions, applying a stress (or strain) on the material changes the Raman frequencies in the material. The change in force constants is represented by a matrix $[\Delta K]$ which can be shown to be symmetric.² The size of this matrix is determined by the degeneracy of the mode. Therefore, for the triply degenerate F_{2g} mode, the $[\Delta K]$ matrix is a 3×3 matrix. The relationship between the $[\Delta K]$ and the applied strain is assumed to be linear and is usually expressed in a form similar to the elastic stress-strain relation described in Eq. (2):

$$\begin{bmatrix} \Delta K_{11} \\ \Delta K_{22} \\ \Delta K_{33} \\ 2\Delta K_{23} \\ 2\Delta K_{13} \\ 2\Delta K_{12} \end{bmatrix} = \begin{bmatrix} \mathbf{K}_{11} & \mathbf{K}_{12} & \mathbf{K}_{12} & 0 & 0 & 0 \\ \mathbf{K}_{12} & \mathbf{K}_{11} & \mathbf{K}_{12} & 0 & 0 & 0 \\ \mathbf{K}_{12} & \mathbf{K}_{12} & \mathbf{K}_{11} & 0 & 0 & 0 \\ 0 & 0 & 0 & \mathbf{K}_{44} & 0 & 0 \\ 0 & 0 & 0 & 0 & \mathbf{K}_{44} & 0 \\ 0 & 0 & 0 & 0 & 0 & \mathbf{K}_{44} \end{bmatrix} \begin{Bmatrix} \epsilon_{11} \\ \epsilon_{22} \\ \epsilon_{33} \\ \epsilon_{23} \\ \epsilon_{13} \\ \epsilon_{12} \end{Bmatrix}_C. \quad (4)$$

\mathbf{K}_{11} , \mathbf{K}_{12} , and \mathbf{K}_{44} are referred to as phonon deformation potentials (PDPs), and for the F_{2g} mode in silicon they are

reported² to have values of $-1.43\omega_0^2$, $-1.89\omega_0^2$, and $-0.59\omega_0^2$, respectively. ω_0 is the Raman frequency of the F_{2g} mode in the unstressed condition and is reported² to be 520 cm^{-1} (as shown in Fig. 1).

(4) It can be shown² that the eigenvalues of the $[\Delta K]$ matrix are related to the Raman frequency shifts as

$$\lambda \equiv 2\omega_0\Delta\omega, \quad (5)$$

where λ denotes the eigenvalues of the $[\Delta K]$ matrix and $\Delta\omega$ represent the shifts in Raman frequency caused by the applied load. The values of λ can be obtained by solving the characteristic equation for $[\Delta K]$ as

$$\det([\Delta K] - \lambda[I]) = 0, \quad (6)$$

where $[I]$ is a unit diagonal matrix. Note that there can be up to three distinct values of λ which correspond to three distinct values of $\Delta\omega$. If all three values of $\Delta\omega$ are distinct, then the initially degenerate F_{2g} mode has split into three singlets. If two of the $\Delta\omega$ values are equal, the mode has split into a singlet and a doublet, and if they all have the same value the mode continues to be triply degenerate.

(5) The relative intensities of the individual peaks can be computed from the relationship

$$I_i \propto |e_s \cdot (\bar{d}_i e_0)|^2, \quad (7)$$

where I_i is the intensity of the individual peak, e_0 is the direction of polarization of the incident beam, and e_s is the direction of polarization selected for the scattered beam. $[\bar{d}]_i$ is the Raman polarizability tensor of the F_{2g} mode in the stressed condition and is different for each of the initially degenerate peaks. $[\bar{d}]_i$ is assumed to be a linear combination of the unstressed polarizability tensors in proportion to the linear combination of the new eigenvectors in terms of the old eigenvectors. In other words, for the F_{2g} mode in silicon

$$[\bar{d}]_i = (n_1)_i [d]_{100} + (n_2)_i [d]_{010} + (n_3)_i [d]_{001}, \quad (8)$$

where $(n_1)_i$, $(n_2)_i$, and $(n_3)_i$, are the directional cosines of the i th eigenvector of the $[\Delta K]$ matrix corresponding to the i th initially degenerate mode, and $[d]_{100}$, $[d]_{010}$, and $[d]_{001}$ are the Raman tensors for the degenerate F_{2g} mode in the unstressed condition. The Raman tensors for the F_{2g} mode in the unstressed condition have been reported¹⁷ as

$$d_1 = \begin{bmatrix} 0 & 0 & 0 \\ 0 & 0 & d \\ 0 & d & 0 \end{bmatrix} d_2 = \begin{bmatrix} 0 & 0 & d \\ 0 & 0 & 0 \\ d & 0 & 0 \end{bmatrix} d_3 = \begin{bmatrix} 0 & d & 0 \\ d & 0 & 0 \\ 0 & 0 & 0 \end{bmatrix}. \quad (9)$$

III. PREDICTION OF UNKNOWN PLANE-STRESS STATES

The previous section described the theoretical computations involved in predicting the peak positions and relative intensities of the initially degenerate F_{2g} peaks in Si wafers in the stressed condition. For a general stress state and selected polarizations of incident and scattered light, the spectra obtained are usually composed of multiple peaks with different intensities. Because there may be up to three overlapping peaks in the combined signal, it is useful to first establish a relationship between the peak position of this

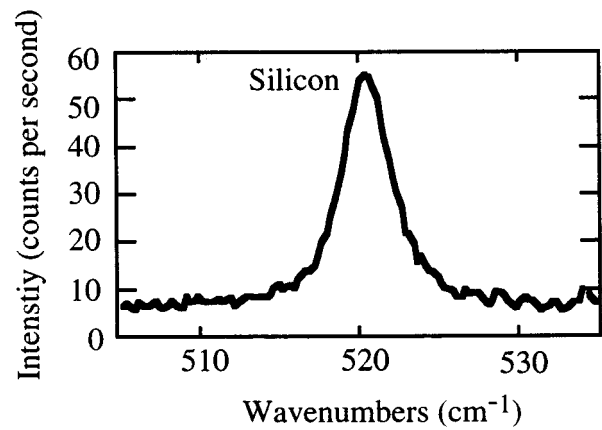


FIG. 1. A typical spectrum showing a silicon peak at around 520 wave numbers.<

combined signal and the peak positions and intensities of the component peaks. Assuming that the individual peak shifts are very small compared to the full width half-maximum (FWHM) of the signal, the “overall” peak shift of the combined signal ($\Delta\bar{\omega}$) can be shown to be the weighted average of the individual peak shifts ($\Delta\omega_i$) with their relative intensities (I_i), i.e.,

$$\Delta\bar{\omega} = \sum_{i=1}^3 \frac{\Delta\omega_i I_i}{I_T}, \quad (10)$$

where I_T represents the total (sum) intensity of the three initially degenerate peaks. Appendix A provides the mathematical derivation of this result assuming that the peak shifts are small and that the intensity distribution of the peak can be represented by a Gaussian distribution¹⁹. It is seen from Eqs. (7)–(9) that the individual peak intensities I_i and the total intensity I_T are functions of the polarization of the incident and scattered beams, and therefore $\Delta\bar{\omega}$ is expected to be a function of the polarization condition. Furthermore, from Eq. (7) it is seen that the intensities are insensitive to interchanging e_0 and e_s because the Raman tensor is symmetric, i.e.,

$$I_i \propto |e_s \cdot (\bar{d} e_0)|^2 = |e_0 \cdot (\bar{d} e_s)|^2. \quad (11)$$

Therefore, there will be a redundancy in the information obtained by changing both e_0 and e_s independently. Due to the inherent advantages with the typical MRS experimental setup used, e_0 (polarization of the incident light) is fixed with respect to the sample reference frame while e_s (polarization of the scattered beam) is systematically varied. The change in $\Delta\bar{\omega}$ with respect to e_s is explored here to determine if the changes are characteristic of the stress state in the wafer. The angle between e_0 and e_s (note that they are both in the same plane for the backscattered geometry shown in Fig. 2) is represented as θ , and is given by

$$\theta = \cos^{-1}(e_0 \cdot e_s). \quad (12)$$

In this study, silicon wafers with a (111) surface were analyzed with the $\langle 1\bar{1}0 \rangle$, $\langle 11\bar{2} \rangle$, and $\langle 111 \rangle$ directions coinciding with the one, two, and three directions, respectively, in the laboratory reference frame (Fig. 3). The direction of

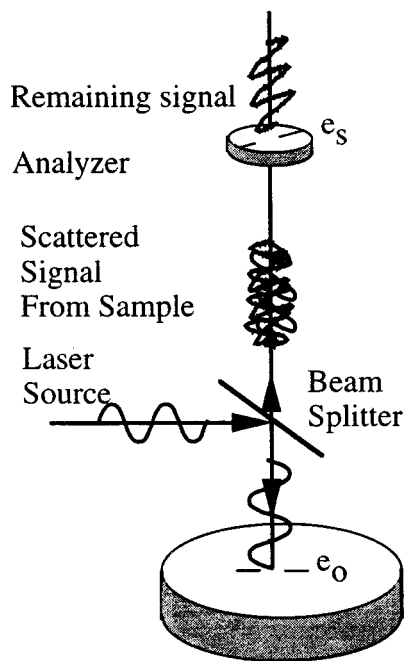


FIG. 2. Schematic representation of the geometry of incident and scattered polarizations. Note that polarization of the incident beam (e_0) and polarization selected using the analyzer (e_s) are in the same plane for the backscattered geometry, and the angle between them is denoted as θ .

polarization of the incident beam (e_0) was fixed along the $\langle 1\bar{1}0 \rangle$ direction (1-axis in laboratory reference frame). The general plane stress state in the (1, 2, 3) frame is represented by

$$[\sigma] = \begin{bmatrix} \sigma_{11} & \sigma_{12} & 0 \\ \sigma_{12} & \sigma_{22} & 0 \\ 0 & 0 & 0 \end{bmatrix}. \quad (13)$$

The computations to determine the functional dependence of $\Delta\bar{\omega}$ on θ for all possible plane-stress states are complex because of the need to find the eigenvectors of the secular determinant [Eqs. (6) and (8)] with three variables. Therefore, it is convenient to break up the general stress state

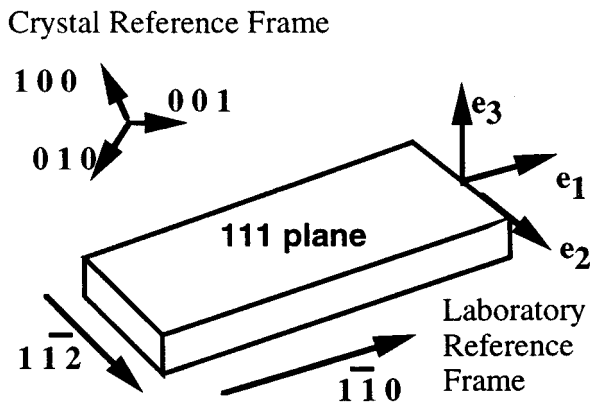
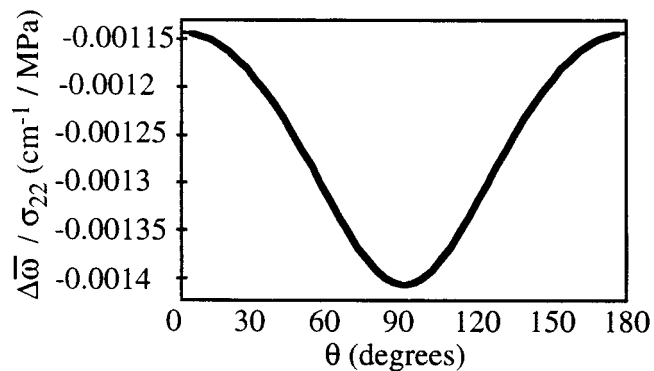
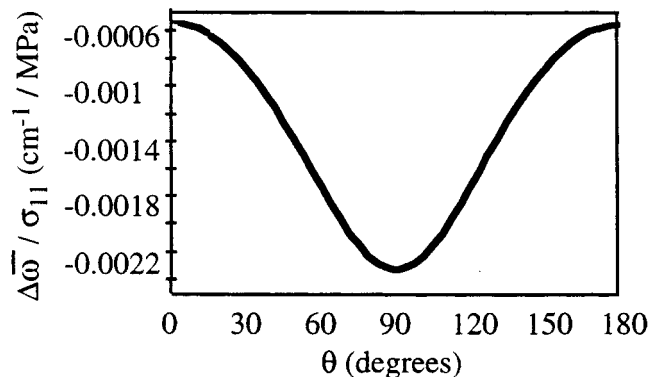


FIG. 3. The geometry of the (111) silicon wafers analyzed in this study. Note the $\langle 1\bar{1}0 \rangle$, $\langle 11\bar{2} \rangle$, and $\langle 111 \rangle$ crystallographic directions have been made to coincide with the 1, 2, and 3 directions in the sample reference frame.



(a)



(b)

FIG. 4. The predicted $\Delta\bar{\omega}/\sigma$ vs θ curves for uniaxial stress in the (111) silicon wafer. (a) Loading along the two direction, (b) loading along the one direction.

in terms of simpler stress states and understand the influence of each of the stress components on the $\Delta\bar{\omega}$ vs θ curve. As the simplest case, consider a stress state where σ_{22} is the only nonzero stress component. For this loading condition, the theory (described in Sec. II) predicts that the three peak shifts $\Delta\omega_i$ are linear with σ_{22} , and that the intensities I_i are independent of σ_{22} . Therefore, $\Delta\bar{\omega}$ is also linear with σ_{22} . A plot of $\Delta\bar{\omega}/\sigma_{22}$ vs θ predicted using the procedures outlined in Sec. II is shown in Fig. 4(a). A similar plot for the case of uniaxial stress along the 1-axis (σ_{11} being the only nonzero stress component) is shown in Fig. 4(b). It will be shown later that the exact shapes of these curves cannot be reproduced by any other stress states. Therefore once these curves are established for the given wafer, they serve to identify the stress components in uniaxial stress states in the selected wafer.

Next, consider a general biaxial stress state, where σ_{11} and σ_{22} are the only nonzero stress components. The $\Delta\bar{\omega}$ vs θ curve for the biaxial state are shown for a range of values of σ_{11} and σ_{22} in Figs. 5(a) and 5(b). It is clear that the curves retain their symmetry (with respect to a θ value of 90°) for all combinations of σ_{11} and σ_{22} . Furthermore, each combination of σ_{11} and σ_{22} produces a distinct curve. In other words, once calibration curves of the type shown in Figs. 5(a) and 5(b) are established for all possible biaxial stress states in the wafer, they can then be used to determine the unknown biaxial stress components for any arbitrary ratio of the biaxial stresses. This by itself, is a significant im-

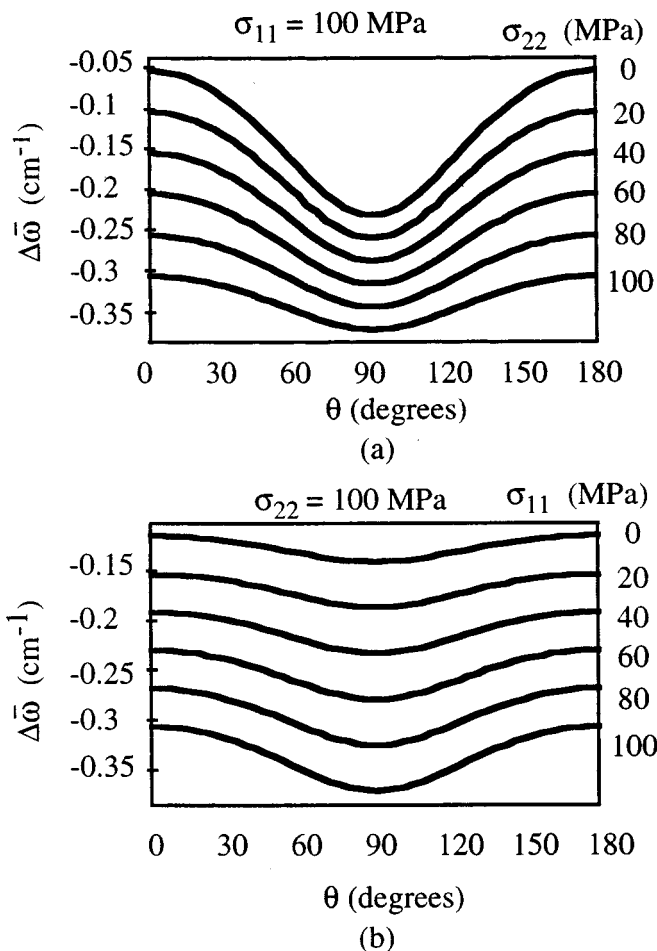


FIG. 5. The variation of the overall peak position in the (111) silicon wafer subjected to a biaxial stress state: (a) fixed σ_{11} and varying σ_{22} , (b) fixed σ_{22} and varying σ_{11} .

provement over currently employed MRS techniques because none of the existing techniques are capable of identifying more than one independent stress component in a multiaxial stress state.

Finally, consider the general plane stress state described in Eq. (13). Figure 6 shows the influence of the shear stress σ_{12} on the $\Delta\bar{\omega}$ vs θ relationship. It is clear that the shear

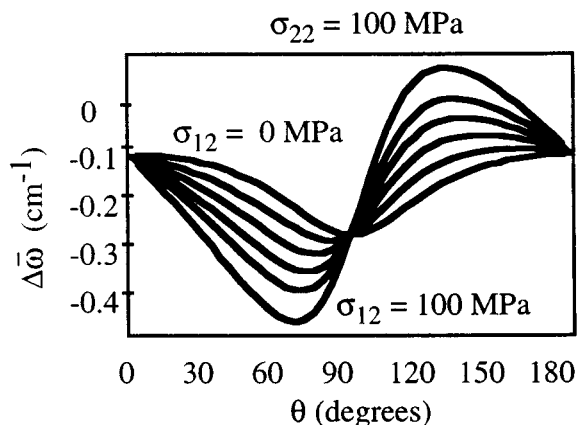


FIG. 6. The variation of the $\Delta\bar{\omega}$ vs θ curves with shear stress for fixed σ_{22} .

stress causes a distinct asymmetry in the $\Delta\bar{\omega}$ vs θ curve (about the θ value of 90°). Note also that the position of the overall peak at 0° and 90° is independent of the shear stress. Thus, it is seen that changing the value of σ_{22} and σ_{11} changes the scale and shape of the $\Delta\bar{\omega}$ vs θ curve while maintaining its symmetry. In contrast, introducing a shear stress changes the symmetry of the curve without changing the values of $\Delta\bar{\omega}$ at 0° and 90° . It was also observed that distinct curves are produced for each set of values of the three stress components. Therefore, in principle, these curves can be used to estimate all three components of the plane stress state in the wafer.

Although, the curves presented in Figs. 5 and 6 indicate that it is possible to determine the general plane stress state from the $\Delta\bar{\omega}$ vs θ curves, it is a very laborious process to establish these curves for all possible values of σ_{11} , σ_{22} , and σ_{12} and then compare the actual measurements with these calibration curves. Because there are three unknown stress components, only three independent values from the $\Delta\bar{\omega}$ vs θ curve are required to determine the unknown stresses. In the technique developed here, these three points have been chosen to correspond to θ values of 0° , 90° , and 60° and are denoted as $(\Delta\bar{\omega})_0$, $(\Delta\bar{\omega})_{90}$, and $(\Delta\bar{\omega})_{60}$, respectively. The first two were chosen because they were observed to be insensitive to shear stress (Fig. 6). Therefore, it should be possible to determine σ_{11} and σ_{22} from these two values alone, independent of the shear stress. $(\Delta\bar{\omega})_{60}$ was chosen as the third point because the $\Delta\bar{\omega}$ vs θ curves in Fig. 5 indicated the highest sensitivity to shear at this point.

It is necessary to establish expressions for the dependence of $(\Delta\bar{\omega})_0$, $(\Delta\bar{\omega})_{90}$, and $(\Delta\bar{\omega})_{60}$, on the three stress components σ_{11} , σ_{22} , and σ_{12} . Because the values for $(\Delta\bar{\omega})_0$ and $(\Delta\bar{\omega})_{90}$ were found to be independent of shear from results shown in Fig. 5, a biaxial stress state was assumed in deriving the expressions for these quantities. The expressions presented here were obtained using the mathematical analysis software MAPLE[®],²⁰ and using the procedures outlined in Sec. II. The expressions derived for $(\Delta\bar{\omega})_0$ and $(\Delta\bar{\omega})_{90}$ are

$$(\Delta\bar{\omega})_0 = \frac{(\mathbf{K}_{11}S_{11} + 2\mathbf{K}_{12}S_{12})\omega_0}{2} \left[-\sigma_{22} \left(\frac{5+7p+q}{12} \right) - \sigma_{11} \left(\frac{1+3p-q}{4} \right) + \Theta \right], \quad (14)$$

$$(\Delta\bar{\omega})_{90} = \frac{(\mathbf{K}_{11}S_{11} + 2\mathbf{K}_{12}S_{12})\omega_0}{2} \left[\sigma_{22} \left(\frac{1+5p-q}{3} \right) + \sigma_{11}(1+p+q) \right], \quad (15)$$

where

$$p = \frac{\mathbf{K}_{11}S_{12} + \mathbf{K}_{12}(S_{11} + S_{12})}{(\mathbf{K}_{11}S_{11} + 2\mathbf{K}_{12}S_{12})}, \quad (16)$$

$$q = \frac{\mathbf{K}_{44}S_{44}}{(\mathbf{K}_{11}S_{11} + 2\mathbf{K}_{12}S_{12})}, \quad (17)$$

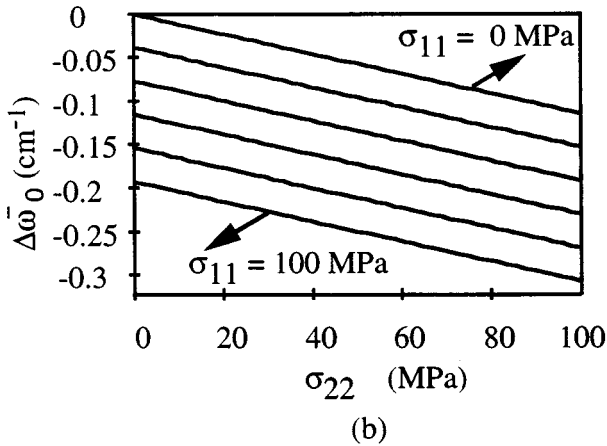
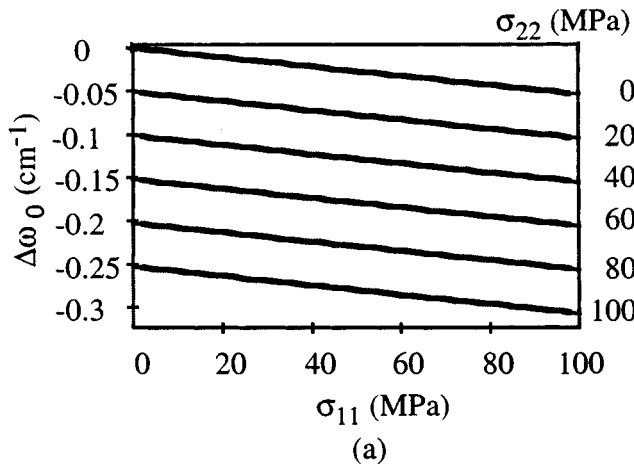


FIG. 7. (a) Plots of $(\Delta\bar{\omega})_0$ vs σ_{11} for different values of σ_{22} . (b) Plots of $(\Delta\bar{\omega})_0$ vs σ_{22} for different values of σ_{11} .

$$\Theta = \frac{\alpha}{36\gamma} \left(\gamma + 4\beta^2 - 2\sqrt{2}q\sigma_{22}\beta - \frac{\sqrt{2}}{3}\alpha\beta \right), \quad (18)$$

$$\alpha = \sqrt{3} \left((3-6p-2q+3p^2+11q^2+2pq) \times \sigma_{22}^2 - 2\sigma_{22}\sigma_{11}(p+q-1)(3p+q-3) + 3\sigma_{11}^2(p+q-1)^2 \right)^{1/2}, \quad (19)$$

$$\beta = -\frac{1}{\sqrt{18}}(p+q-1)(\sigma_{22}-\sigma_{11}), \quad (20)$$

$$\gamma = \frac{1}{144} \left(\sqrt{18}\beta - 6q\sigma_{22} - \alpha \right)^2 + \beta^2. \quad (21)$$

Because Eqs. (14) and (15) are equations in two unknowns, it is possible to determine σ_{11} and σ_{22} in a general plane stress state from just two measurements, $(\Delta\bar{\omega})_0$ and $(\Delta\bar{\omega})_{90}$, provided all the material constants are known. If the values of the material constants (elastic compliances and PDPs) are not known, the relationships for $(\Delta\bar{\omega})_0$ and $(\Delta\bar{\omega})_{90}$ can be established experimentally. It is evident from Eq. (15) that $(\Delta\bar{\omega})_{90}$ is linear in both σ_{11} and σ_{22} . Although the analytical expression in Eq. (14) indicates a nonlinear dependence of $(\Delta\bar{\omega})_0$ on σ_{11} and σ_{22} , plots of $(\Delta\bar{\omega})_0$ vs σ_{11} for different values of σ_{22} and plots of $(\Delta\bar{\omega})_0$ vs σ_{22} for different values of σ_{11} are essentially linear as shown in

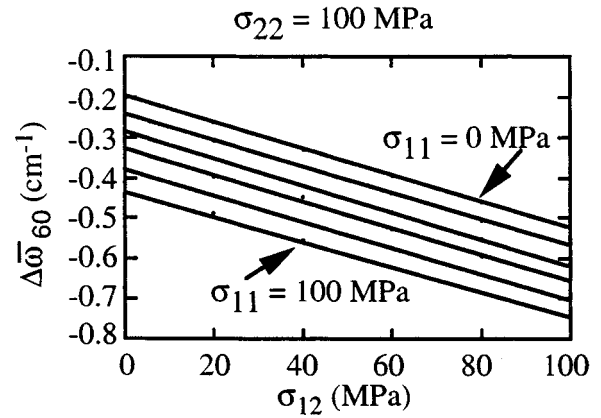


FIG. 8. A typical plot of $(\Delta\bar{\omega})_{60}$ vs σ_{12} for given values of σ_{11} and σ_{22} .

Figs. 7(a) and 7(b) (at least in the range of stresses encountered in this study). Because the slopes of the lines in each of these plots do not appear to change with the stress values, it can be inferred that the dependence of $(\Delta\bar{\omega})_0$ on σ_{11} and σ_{22} is essentially linear. Therefore, the relationships for $(\Delta\bar{\omega})_0$ and $(\Delta\bar{\omega})_{90}$ in terms of σ_{11} and σ_{22} can be expressed approximately as

$$(\Delta\bar{\omega})_0 = a\sigma_{11} + b\sigma_{22}, \quad (22)$$

$$(\Delta\bar{\omega})_{90} = c\sigma_{11} + d\sigma_{22}. \quad (23)$$

The unknowns, a , b , c , and d , can be established experimentally by applying known stresses on the Si wafer in the one and two directions.

Once σ_{11} and σ_{22} are determined in a given Si wafer, the value of σ_{12} can be estimated from a measurement of $(\Delta\bar{\omega})_{60}$. Note that the value of $(\Delta\bar{\omega})_{60}$ depends on all three stress components. A typical plot of $(\Delta\bar{\omega})_{60}$ vs σ_{12} for given values of σ_{11} and σ_{22} , shown in Fig. 8, indicates that the slope is independent of the values of σ_{11} . A similar plot of $(\Delta\bar{\omega})_{60}$ vs σ_{12} for varying values of σ_{22} indicated that the slope of the lines in Fig. 8 is also independent of σ_{22} . Since the effects of the shear and normal components are found to be independent for the (111) wafer, they can be decoupled from each other. Thus, $(\Delta\bar{\omega})_{60}$ can be expressed as

$$(\Delta\bar{\omega})_{60} = \bar{h}(\sigma_{11}, \sigma_{22}) + \chi\sigma_{12}, \quad (24)$$

where \bar{h} is a function independent of shear stress and χ is a constant independent of σ_{11} and σ_{22} . The biaxial stress state was used to determine the function \bar{h} in terms of σ_{11} and σ_{22} and a pure shear stress state was used to determine the value of χ . These expressions were found using MAPLE^{®20} and are summarized as:

$$(\Delta\bar{\omega})_{60} = \frac{(\mathbf{K}_{11}S_{11} + 2\mathbf{K}_{12}S_{12})\omega_0}{2} \left[-\sigma_{22} \left(\frac{1-13p+5q}{24} \right) + \sigma_{11} \left(\frac{3+p+5q}{8} \right) + \frac{\Theta}{2} \right] + \chi\sigma_{12}, \quad (25)$$

where

$$\chi = \frac{\mathbf{K}_{11} S_{11} \omega_0 \mu \sqrt{3}}{72 q^2 (1+p+\mu)^2} (\rho - 2\sqrt{2} q \mu + 4p - 2q^2) \times [\rho + 2(\sqrt{2} + \sqrt{6}) q (p+1) - 2\sqrt{6} q \mu + 2q^2], \quad (26)$$

$$\rho = p^2 - p\mu + \mu - 1, \quad (27)$$

$$\mu = 1 - 2p + p^2 + 2q^2, \quad (28)$$

and p , q , and Θ were defined in Eqs. (16)–(18). Once the values of σ_{22} and σ_{11} are determined from Eqs. (14) and (15) [or equivalently from Eqs. (22) and (23)], the value of the shear stress component can be determined from Eq. (25).

It is also possible to establish the relationship in Eq. (25) from experiments. Plots of $(\Delta\bar{\omega})_{60}$ vs σ_{22} for given values of σ_{12} and σ_{11} and plots of $(\Delta\bar{\omega})_{60}$ vs σ_{11} for given values of σ_{12} and σ_{22} also indicated linear relationships (similar to those seen in Fig. 8). It is therefore reasonable to assume a linear relationship of $(\Delta\bar{\omega})_{60}$ with σ_{11} and σ_{22} (in the function \bar{h}). $(\Delta\bar{\omega})_{60}$ can therefore be approximated to be linear with all three stress components as

$$(\Delta\bar{\omega})_{60} = e\sigma_{11} + f\sigma_{22} + g\sigma_{12}. \quad (29)$$

The constants e , f , and g can be determined by measuring the values of $(\Delta\bar{\omega})_{60}$ from three different experiments where the stress states correspond to tension in the one direction, tension in the two direction, and shear in the 1–2 plane, respectively. With these expressions [Eqs. (22), (23), and (29)], it is possible to determine σ_{12} , once the values of σ_{11} and σ_{22} have been estimated.

The technique proposed here for determining the three unknown plane stress components in (111) Si wafers can be summarized as follows.

Step 1: Align the incident beam parallel to $\langle 1\bar{1}0 \rangle$ and take spectra at the desired location on the wafer with the analyzer rotated at 0° , 60° , and 90° relative to the polarized incident beam.

Step 2: Curve fit the peaks to a Gaussian distribution and evaluate the shift in the overall peak position from the unstressed condition, for the three angles. Denote these as $(\Delta\bar{\omega})_0$, $(\Delta\bar{\omega})_{60}$, and $(\Delta\bar{\omega})_{90}$.

Step 3: Find the values of σ_{11} and σ_{22} from expressions (14) and (15) by solving the two simultaneous equations [or using the equivalent relations (22) and (23) established experimentally].

Step 4: Determine the value of σ_{12} from expression (25) [or the equivalent relation (29) established experimentally].

The main assumption in this approach is the relation derived for the peak position of the combined signal in terms of the individual peak positions and intensities [Eq. (10)]. In deriving this relation (Appendix A) the peak shape was assumed to be a Gaussian because the peak shape obtained for the silicon peaks from the experimental setup appears to be a Gaussian (as shown in Fig. 1). The approximation to ignore higher order terms in the expansion for the exponent in Eq. (A2) is valid within the stress ranges encountered in electronic structures. In order to evaluate critically the error introduced by these approximations, the ratio of the peak position of the combined signal calculated using Eq. (10) to the peak position of the combined signal without the approxima-

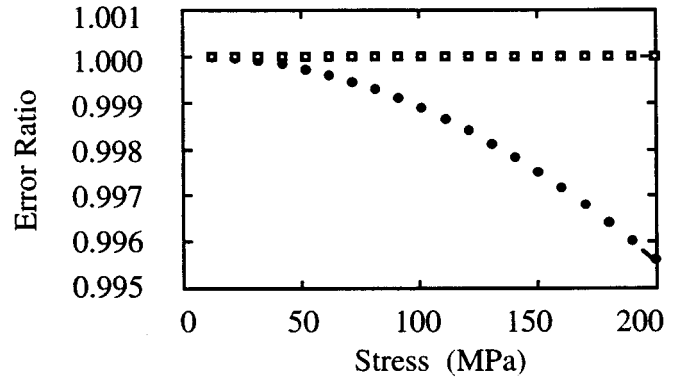


FIG. 9. Plots showing the variation of the error ratio with the applied stress (■) represents the curve for a uniaxial stress (σ_{22}) where the component peaks were assumed to be Gaussian, (●) represents the curve for a shear stress (σ_{12}) assuming Gaussian peaks, and (○) represents the curve for the uniaxial stress where the component peaks were assumed to be Lorentzian. (Note that the curves with (■) and (○) overlap.)

tion was defined as the “error” ratio. A significant deviation of the value of this error ratio from 1.0 would indicate that Eq. (10) is no longer valid. Figure 9 shows the variation of the error ratio for two different stress states—a uniaxial stress and a shear stress. For the case of a uniaxial stress, the error ratio remains very close to 1.0 (with a change only in the sixth decimal place) for stresses up to 200 MPa. For the case of a shear stress, the error ratio approaches 0.995 for a shear stress of about 200 MPa. It should be noted that the stresses encountered in electronic structures are typically well below 150 MPa, and therefore the above analyses indicate that the procedures described in this paper can be applied without impunity. The different behavior of the error ratio in the uniaxial stress condition and in the shear stress condition (Fig. 9) is due to the different ways the individual components of the Raman signal shift as a consequence of the applied stress. In uniaxial stress all of the component modes shift in the same direction, whereas in the shear stress the component modes shift in opposite directions. Consequently, the component modes are relatively farther apart in the shear case than in the uniaxial stress case. Therefore, there is a higher deviation of the error ratio from a value of 1.0 in the shear case. In fact, the error ratio for the uniaxial case remains very close to 1.0 even up to stresses of 4000 MPa when it reaches a value of about 0.99.

Figure 9 also shows the error ratio obtained if a Lorentzian line shape was assumed instead of the Gaussian line shape. It is observed that the results were essentially unaffected by this change. This is because the peak shifts here are extremely small compared to the full width half-maximum of the signals typically obtained in these measurements. In fact, as explained earlier, that is the reason why the individual modes could not be decoupled by mathematical analyses, and there arose a need to develop the procedures described in this paper.

This approach of using the shape and scale of the $\Delta\bar{\omega}$ vs θ curve for determining the unknown in-plane stress components is successful, at least theoretically, in the case of a (111) Si wafer. This does not imply, however, success for the method in wafers with any orientation. For example, the

$\Delta\bar{\omega}$ vs θ curve for the (001) Si wafer showed that only the tensile components can be determined by this technique (for a backscattered geometry and e_0 fixed in the $\langle 010 \rangle$ direction), i.e., the curve is insensitive to the shear stress. Although measuring two stress components is better than determining only the stress magnitude, other approaches are necessary to determine all three stress components for the (100) wafer. Geometries other than the backscattered geometry in combination with the type of technique developed here should provide a way to estimate all the stress components in such cases.

IV. CONCLUSIONS

A new approach to determining all three unknown plane-stress components in (111) silicon wafers has been devised based on analyzing the position of the “combined Raman signal” (corresponding to the initially degenerate F_{2g} peaks) as a function of the relative angle between the polarized incident beam and the angle of the analyzer, which allows us to selectively observe the components in the scattered beam. It was found that the curve for the overall shift per unit stress as a function of the relative angle holds all information necessary to determine the stress state and the magnitude of the stress components. Analytical expressions are given for the position of the combined signal at three angles (0° , 60° , and 90°) and based on these three values an algorithm is devised to estimate the magnitudes of the stress components in plane stress loading of (111) silicon wafers.

ACKNOWLEDGMENTS

The authors would like to thank NSF, Civil and Mechanical Systems (Grant No. MSS 9402692) and NSF Division of Materials Research, NYI Program for supporting this research. We would like to acknowledge Mark A. Shiber and Dr. Fran Adar of Instruments SA for useful discussions.

APPENDIX A

The Gaussian distribution function for a peak with center ω_i , can be expressed as

$$I_i(\omega) = I_i e^{-(\omega - \omega_i/\sigma)^2}, \quad (\text{A1})$$

where I_i is the intensity of the signal. Assuming the exponent in (A1) is $\ll 1$ (in the close vicinity of the peak), the intensity distribution function can be approximated as

$$I_i(\omega) = I_i \left[1 - \left(\frac{\omega - \omega_i}{\sigma} \right)^2 \right]. \quad (\text{A2})$$

Assuming small shifts of the three initially degenerate

peaks, the intensity of the combined signal can be expressed as

$$\begin{aligned} \sum_{i=1}^3 I_i(\omega) &= \sum_{i=1}^3 I_i \left[1 - \left(\frac{\omega - \omega_i}{\sigma} \right)^2 \right] \\ &= I_T - \frac{1}{\sigma^2} \sum_{i=1}^3 I_i (\omega - \omega_i)^2, \end{aligned} \quad (\text{A3})$$

where, $I_T = \sum_{i=1}^3 I_i$.

Replacing ω_i with $\omega_0 + \Delta\omega_i$, (A3) can be rewritten as

$$\sum_{i=1}^3 I_i(\omega) = I_T - \frac{1}{\sigma^2} \sum_{i=1}^3 I_i (\omega - \omega_0 - \Delta\omega_i)^2. \quad (\text{A4})$$

The point of maximum intensity for the combined signal can be identified by solving

$$\left[\frac{d}{d\omega} \left(\sum_{i=1}^3 I_i(\omega) \right) \right]_{\omega=\bar{\omega}} = 0 \quad (\text{A5})$$

and can be expressed as

$$\Delta\bar{\omega} = \bar{\omega} - \omega_0 = \sum_{i=1}^3 \frac{I_i \Delta\omega_i}{I_T}. \quad (\text{A6})$$

- ¹H. A. Szymanski, *Raman Spectroscopy, Theory and Practice* (Plenum, New York 1967), Vols. 1 and 2.
- ²E. M. Anastassakis, in *Dynamical Properties of Solids*, edited by G. K. Horton, and A. A. Maradudin (North Holland, Amsterdam, 1980).
- ³E. Anastassakis and E. Liarokapis, *J. Appl. Phys.* **62**, 3346 (1987).
- ⁴K. Yamazaki, M. Yamada, K. Yamamoto, and K. Abe, *Jpn. J. Appl. Phys.*, Part 1 **23**, 681 (1984).
- ⁵T. Ito, H. Azuma, and S. Noda, *Jpn. J. Appl. Phys.*, Part 1 **33**, 171 (1994).
- ⁶S. Nakashima, Y. Inoue, M. Miyauchi, A. Mitsuishi, T. Nishimura, T. Fukumoto, and Y. Akasaka, *J. Appl. Phys.* **54**, 2611 (1983).
- ⁷J. Vanhellemont, I. De Wolf, K. G. F. Janssens, S. Frabboni, R. Balboni, and A. Armigliato, *Appl. Surf. Sci.* **63**, 119 (1993).
- ⁸N. Melanitis and C. Galiotis, *Proc. R. Soc. London, Ser. A* **440**, 379 (1993).
- ⁹M. C. Andrews, R. J. Day, X. Hu, and R. J. Young, *Composite Sci. Technol.* **48**, 255 (1993).
- ¹⁰X. Yang and R. J. Young, *Composites* **25**, 488 (1994).
- ¹¹E. Anastassakis, A. Pinczuk, E. Burstein, F. H. Pollack, and M. Cardona, *Solid State Commun.* **8**, 133 (1970).
- ¹²I. De Wolf, J. Vanhellemont, A. Romano-Rodriguez, H. Norstrom, and H. E. Maes, *J. Appl. Phys.* **71**, 898 (1992).
- ¹³P. Gans and J. B. Gill, *Appl. Spectrosc.* **31**, 451 (1977).
- ¹⁴J. F. Degregorio, T. E. Furtak, and J. J. Petrovic, *J. Appl. Phys.* **71**, 3524 (1992).
- ¹⁵K. E. D. Sumanasiri and O. Van der Biest, *Scr. Metall. Mater.* **30**, 79 (1994).
- ¹⁶H. Sakata, G. Dresselhaus, M. S. Dresselhaus, and M. Endo, *J. Appl. Phys.* **63**, 2769 (1988).
- ¹⁷R. Loudon, *Adv. Phys.* **13**, 423 (1964).
- ¹⁸G. Simmons and H. Wang, *Single Crystal Elastic Constants and Calculated Aggregate Properties: A Handbook* (MIT, Cambridge, MA, 1971).
- ¹⁹A. Baruya and W. F. Maddams, *Appl. Spectrosc.* **32**, 563 (1978).
- ²⁰MAPLEV© Student Edition (Brooks Cole Publishing, CA, 1981).